Live Imaging of Telomeres: yKu and Sir Proteins Define Redundant Telomere-Anchoring Pathways in Yeast

Florence Hediger, Frank R. Neumann,
Griet Van Houwe, Karine Dubrana,
and Susan M. Gasser[1]
University of Geneva
Department of Molecular Biology
Quai Ernest-Ansermet 30
CH-1211 Geneva 4
Switzerland

Summary

Background: The positioning of chromosomal domains within interphase nuclei is thought to facilitate transcriptional repression in yeast. Although this is particularly well characterized for telomeres, the molecular basis of their specific subnuclear organization is poorly understood. The use of live fluorescence imaging overcomes limitations of in situ staining on fixed cells and permits the analysis of chromatin dynamics in relation to stages of the cell cycle.
Results: We have characterized the dynamics of yeast telomeres and their associated domains of silent chromatin by using rapid time-lapse microscopy. In interphase, native telomeres are highly dynamic but remain within a restricted volume adjacent to the nuclear envelope. This constraint is lost during mitosis. A quantitative analysis of selected mutants shows that the yKu complex is necessary for anchoring some telomeres at the nuclear envelope (NE), whereas the myosin-like proteins Mlp1 and Mlp2 are not. We are able to correlate increased telomeric repression with increased anchoring and show that silent chromatin is tethered to the NE in a Sir-dependent manner in the absence of the yKu complex. Sir-mediated anchoring is S phase specific, while the yKu-mediated pathway functions throughout interphase. Subtelomeric elements of yeast telomere structure influence the relative importance of the yKu- and Sir-dependent mechanisms.
Conclusions: Interphase positioning of telomeres can be achieved through two partially redundant mechanisms. One requires the heterodimeric yKu complex, but not Mlp1 and Mlp2. The second requires Silent information regulators, correlates with transcriptional repression, and is specific to S phase.

Introduction

Chromatin assumes a nonrandom distribution in interphase nuclei (reviewed in [1]). The function of its spatial arrangement is largely unknown, although recent evidence suggests that subnuclear compartments contribute to the establishment and maintenance of epigenetic controls over gene expression [2, 3]. This has been particularly well characterized at yeast telomeres, which nucleate the formation of a compact chromatin structure

[1]Correspondence: susan.gasser@molbio.unige.ch

that represses the transcription of adjacent RNA pol II genes in a heritable fashion (termed telomeric position effect, or TPE [4, 5]). This silent subtelomeric chromatin is found clustered near the nuclear envelope (NE) in discrete foci [6–10]. Telomeres of the parasite *Plasmodia* also tend to cluster near the nuclear periphery, an organization that may favor gene conversion between members of subtelomeric virulence factor loci [11].

Telomeres have a repetitive sequence organization that ensures the stability of eukaryotic genomes by protecting the ends of linear chromosomes from degradation and fusion events. Most eukaryotic telomeres consist of both a terminal TG-rich repeat and larger middle-repetitive subtelomeric elements (reviewed in [12]). In budding yeast, ~300 bp of an irregular TG repeat (abbreviated $[TG_{1–3}]_n$) is sufficient to ensure the protection and replication of chromosomal ends and to nucleate the formation of silent chromatin, while the function of the larger subtelomeric repeats, X and Y′, remains unclear. The presence of insulator elements within the yeast elements suggests that they may protect nearby genes from TPE [13, 14], while *Drosophila* subtelomeric repeats can induce variegated patterns of repression on integrated reporters [15].

The initial observation that budding yeast telomeres form foci adjacent to the NE was based on immunostaining of the telomeric repeat binding protein Rap1p and structural proteins of repressed chromatin, the Silent Information Regulators Sir3p and Sir4p [7, 10]. These punctate staining patterns are lost under a range of conditions that perturb TPE (reviewed in [2]). However, because telomeres remained largely perinuclear in silencing-deficient *sir* mutants, it was concluded that the peripheral anchoring of telomeric sequences can occur independently of transcriptional repression [10, 16]. This finding argued that a perinuclear position is not sufficient to confer repression on genes. Nonetheless, it was thought likely that telomere clustering might promote repression by creating zones with critically high concentrations of silencing factors [10, 17].

The major structural component of silent chromatin in budding yeast is a histone tail binding complex composed of three unrelated proteins, Sir2, Sir3, and Sir4. These also serve to repress the cryptic mating type loci *HML* and *HMR*, situated 12 and 25 kb from the left and right telomeres, respectively, of chromosome III (reviewed in [18]). Because normal cellular Sir protein concentrations are limiting for repression [19–21], it was proposed that juxtaposition of reporter genes to telomeric pools of Sir factors might promote silencing. Indeed, silent mating cassettes or silencer-flanked reporters placed far from telomeres are not silent under normal conditions but can be repressed when Sir factors are delocalized from telomeres, confirming that telomeric foci sequester Sir factors from potential sites of action [21–24]. Consequently, it was shown that Sir-mediated repression at internal silencers can be improved by tethering the reporter to the nuclear envelope through a membrane-associated anchor [17].

Maintenance of both TPE and the telomere-associated pools of Sir factors requires a highly conserved end binding heterodimer, yKu70/80 (reviewed in [25]). This multifunctional complex is essential for the repair of double-strand breaks by nonhomologous DNA end joining [26], yet it also shields native ends from degradation and fusion [27] and may contribute to telomerase recruitment in yeast [28]. Importantly, FISH studies using a Y′ and [TG$_{1-3}$] probe show that the perinuclear anchoring of telomeres is partially compromised in yKu mutants (i.e., deletions of *HDF1* or *HDF2* [8, 24]).

The Ku complex binds to terminal [TG$_{1-3}$]$_n$ sequences independently of the telomere's silencing status [27] but associates with repressed subtelomeric chromatin in a Sir-dependent manner [29]. Like Rap1p, yKu nucleates repression through interaction with Sir4p when targeted to internal reporter genes and can therefore help recruit Sir complexes to telomeres [29]. A recent report shows that yKu70p binds a nuclear myosin-like protein, Mlp2p [30], a member of a conserved family of coiled-coil proteins that is found along the inner face of the NE in yeast [31]. These workers propose that yeast telomeres are attached to pores through the yKu-Mlp interaction [30]. On the other hand, it was previously shown that Y′ FISH signals do not colocalize with the staining of integral pore components [10] and that telomeres fail to relocalize when pores shift to one side of the nucleus in a *nup133* mutant [32].

To resolve the discrepancies concerning the mechanisms of yeast telomere anchoring, we have tagged native chromosomal ends with binding sites for a GFP-*lac* repressor fusion, allowing us to characterize the position and dynamics of telomeres in living yeast cells [33–36]. Using strains lacking yKu and Sir proteins, we identify two partially redundant pathways for telomere anchoring and show that neither requires Mlp1 or Mlp2. Surprisingly, the two tethering mechanisms differ in their relative efficiency in G1 and S phases of the cell cycle and in their relative importance at different telomeres. The Sir-dependent anchoring pathway allows a means for repressed chromatin to position itself autonomously within the nucleus, mechanistically linking telomere localization with transcriptional silencing in vivo.

Results

Quantitation of the Subnuclear Position of Yeast Telomeres in Living Cells

The labeling of budding yeast telomeres with Y′ and [TG$_{1-3}$]$_n$ FISH in interphase cells, coupled with counterstaining for nuclear pores and/or telomeric proteins, suggested that the 32 telomeres cluster in 6–8 foci [10]. Roughly 70% of these foci could be mapped to a peripheral zone corresponding to half the nuclear volume [10, 33]. Quantitative analysis of a truncated, GFP-tagged telomere in fixed cells stained for the nuclear envelope gave similar results [16]. These approaches provided a snapshot view of a population of cells at a given time point but could not resolve whether only a subset of telomeres are anchored (e.g., 30% of all telomeres are stably internal), or if positions are simply very dynamic (e.g., that a given telomere is peripheral 70% of the time).

In addition, because spheroplasting impairs analysis of bud presence and size, changes due to cell cycle progression could not be accurately monitored. Fluorescence imaging of a GFP-*lac* repressor fusion bound to an array of *lac* operator sites (*lac*^{op}; [34]) inserted in subtelomeric sequences allows visualization of individual telomeres in living cells. Coexpression of a nuclear pore-GFP fusion permits a cell-by-cell analysis of telomere position with respect to the NE and allows assignment of cell cycle stages based on bud size and nuclear shape [33].

Using these methods, telomeres (Tel) VI-R, XIV-L and VIII-L were tagged with *lac*^{op} sequences without altering their native subtelomeric repeats (Figure 1A), and three-dimensional (3D) focal stacks of growing yeast cells were scored for telomere position. Their distribution in G1, early S (eS), and mid-to-late S (mlS) phases of the cell cycle is shown in Figure 1. To calculate the position of the telomere relative to the nuclear periphery, telomere-to-pore distances were scored in the focal plane with the brightest GFP-*lac* repressor signal. This value was divided by the nuclear diameter in that particular focal plane, and the ratio was scored relative to three zones of equal surface (Figures 1A and 1B). If a given telomere were randomly distributed in the nucleus, it would be found with equal frequency (33%) in each zone, which is the case for several *lac*^{op}-tagged internal chromosomal domains ([33] and Figure S1 [see the Supplementary Material available with this article online]).

In G1 phase, all three native telomeres show a significant enrichment in the peripheral-most zone (zone I), which has a width of only ∼0.18 μm (0.184 × r). The percentage of telomeres found within zone I ranges from 49% to 71% in early S phase, values significantly higher than those expected for a random distribution (see legend of Figure 1 for χ^2 analysis and p values, n > 200 for each strain). The efficiency of anchoring varies from telomere to telomere but does not correlate strictly with the length of the chromosome arm or with the presence or absence of Y′ elements or STR, an X-associated repeat with antisilencing effects (based on published sequences and unpublished results, Figure 1A). Indeed, Tel VI-R, which has neither element, and Tel XIV-L, which has both, have similar distributions, while Tel VIII-L, which also has both elements, is weakly anchored in G1 and mid-to-late S phases (Figure 1B).

Telomere Dynamics in Interphase and Mitosis

Rapid time-lapse confocal microscopy of the GFP-tagged Tel VI-R allows us to further characterize the spatial constraints imposed on yeast telomeres. As previously demonstrated, 300–400 sequential images can be acquired at 1.5-s intervals without a detectable impact on the immediate cell division cycle [35]. Time-lapse analysis shows that Tel VI-R is not immobile at the nuclear periphery, but that it moves back and forth along the NE, occasionally moving into the nucleoplasm (see Movie 1 showing Tel VI-R in G1 phase in the Supplementary Material). This is in contrast to an integral membrane component such as the spindle pole body (SPB), which remains continuously associated with the pore signal [35]. Although a sporadic deformation of the NE
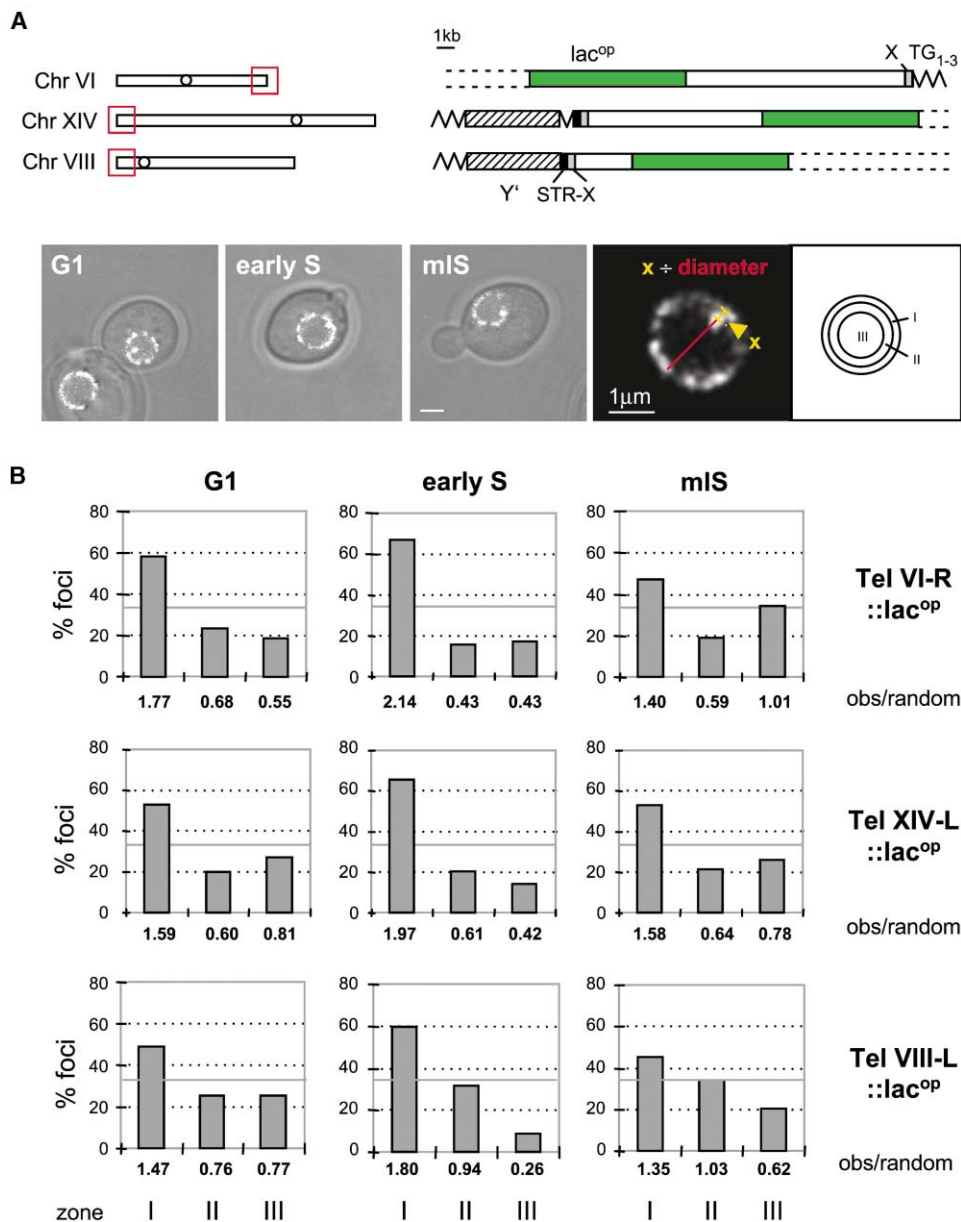
A

B

Figure 1. Individual Yeast Telomeres Are Enriched at the Nuclear Periphery

(A) Telomeres VI-R, XIV-L, and VIII-L were tagged by inserting ~150 *lac* operators at 14, 19, and 11 kb from the indicated chromosomal end in the haploid wild-type strain, GA-1320 [33]. Subtelomeric elements (X, STR, and Y′, indicated by appropriately shaded boxes) and $[TG_{1-3}]_n$ repeats (black zig-zag) remain intact. The *lac*op array is visualized by binding a GFP-*lac* repressor fusion, and the nuclear envelope is visualized through a Nup49-GFP fusion. Typical single-plane confocal images for G1, early S (eS), and mid-to-late S (mIS) phase cells are shown. Spot to the middle of the pore signal (yellow) measurements are described in the Experimental Procedures, and once divided by the nuclear diameter (red), the GFP spot position can be mapped to one of three concentric zones of equal surface.

(B) For each stage of the cell cycle, G1, early S (eS), and mid-to-late S phase (mIS), data are represented in bar graphs as the percentage of spots (*y* axis) per zone (*x* axis). The horizontal bar at 33% corresponds to a random distribution. The fold enrichment or depletion in comparison to randomness is indicated at the bottom of each column. The number of cells analyzed and the confidence values (p) for the χ^2 analysis between random and test distributions are indicated here in parentheses for each cell cycle stage (G1; eS; mIS): Tel VI-R::*lac*op (110, p = 6.2 × 10^{-8}; 49, p = 1.1 × 10^{-7}; 86, p = 9.9 × 10^{-3}), Tel XIV-L::*lac*op (257, p = 8.1 × 10^{-11}; 64, p = 2.5 × 10^{-7}; 89, p = 4.4 × 10^{-4}), Tel VIII-L::*lac*op (218, p = 5.2 × 10^{-6}; 35, p = 9.4 × 10^{-4}; 87, p = 2.2 × 10^{-2}).

contributes to the dynamics of both the SPB and Tel VI-R, by measuring distances from the center of intensity of the GFP-*lac* repressor spot to the middle of the nearest pore signal, we can monitor radial movements that are independent of NE deformation. Tel VI-R is seen to make oscillating movements of 150–300 nm, suggesting a reversible interaction with NE components (Figure 2A; see Movies 1 and 2 in the Supplementary Material). Larger radial movements (>0.5 μm within a 10.5-s window, see red boxes), which are readily scored for internal
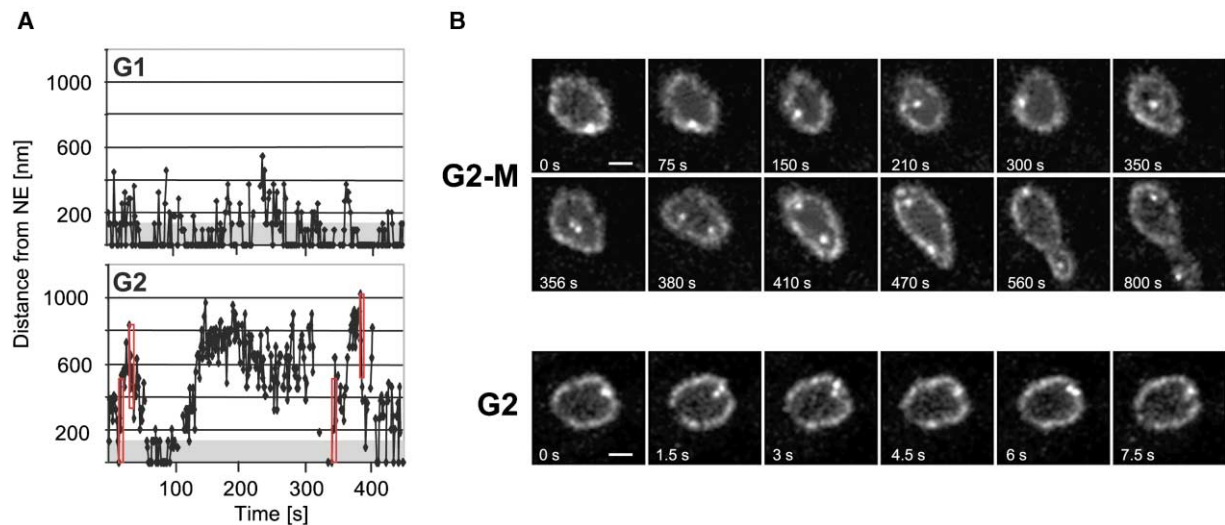
A

B

Figure 2. Dynamics of Tel VI-R during the Cell Cycle

(A) Radial movement of the GFP-tagged Tel VI-R relative to the nuclear envelope (NE) was monitored by measuring the distance from the middle of the spot to the middle of the pore signal in each frame of a typical 450 s time-lapse series from G1 or G2 cells. Distances in nm from the pore signals are plotted against time. The shaded zone at the bottom of the graph represents half of the average width of the pore signal (135 nm) and indicates the zone in which telomere and pore signals are indistinguishable. Red boxes indicate radial movements >0.5 μm within 10.5-s intervals.

(B) In the upper panel, 12 selected confocal images from a typical time-lapse series of GA-1459 during G2-M, taken at 1.5-s intervals with a Zeiss LSM510 confocal microscope over a 5-min period, are shown. Complete 5-min time-lapse series for tagged Tel VI-R in G1, S, and G2-M cells are contained in the Supplementary Material. The mobility and displacement of the GFP-tagged telomere relative to NE are particularly visible in frames between 210 s and 470 s. The scale bar represents 1 μm. The lower panel is the same as the upper panel, but sequential confocal images captured at 1.5-s intervals in a late G2 phase cell are shown. The separation or breathing of the two replicated Tel VI-R signals is seen as a doublet that remains perinuclear. The scale bar represents 1 μm.

tagged sites (10 ± 3 per 10 min; see [35]) occur only once per 10 min for the telomere in G1 phase. On the other hand, Tel VI-R becomes significantly more mobile in G2 phase cells (Figure 2A; see Movie 3 in the Supplementary Material).

Time-lapse analyses of Tel VI-R in cells passing through mitosis show that the telomere is "released" from the nuclear periphery as the nucleus extends into the daughter cell (see frame 350 s, Figure 2B, and time-lapse series mitosis in the Supplementary Material). The release of the telomere from perinuclear constraints co-incides with a partial redistribution of telomeric proteins [9]. It does not, however, necessarily precede telomere replication: time-lapse imaging reveals an increase in GFP intensity and a separation of the Tel VI-R signal into two oscillating spots without significant displacement from the nuclear periphery (Figure 2B).

Loss of yKu, but Not of Myosin-like Proteins, Releases Tel VI-R from the Periphery

If NE anchoring reflects the presence of a telomere-specific ligand, rather than the exclusion of telomeres from a nuclear core, then the disruption of such a ligand should alter telomere position. As discussed above, Y' FISH analyses in mutant cells suggest two sets of factors that might influence telomere anchoring in vivo; the first is the yKu complex [8], and the second involves the myosin-like proteins Mlp1 and Mlp2 [37]. Because partial effects were detected by Y' FISH in both cases [8, 37], we have monitored Tel VI-R dynamics live and have

introduced complete disruptions of the gene encoding yKu70 (hdf1) or the two related *MLP* genes (mlp1 and mlp2 [mlp1 mlp2]) in the lac^{op}-tagged strain.

Focal stacks of exponentially dividing cells were scored for Tel VI-R position relative to the NE as in Figure 1. In the *hdf1* mutant, Tel VI-R loses the enrichment found in wild-type (wt) cells for the peripheral-most zone and assumes a random distribution at all stages of interphase, as confirmed by χ^2 analysis (Figure 3A legend shows that the *hdf1* Tel VI-R distribution is statistically indistinguishable from a random distribution). This distribution is also clearly distinct from that in wt cells (p = 3.4×10^{-7}, 1.8×10^{-2}, 7.4×10^{-2} for G1, eS, and mIS, respectively). Importantly, there is no change in the average nuclear diameter in mutant cells (∅ in G1 is 1.89 μm in *hdf1*, n = 168, σ = 0.23 versus 1.86 μm in wt cells, n = 110, σ = 0.23), and the effect of the *hdf1* mutation is specific for telomeres, as there is no shift from the perinuclear zone I of a nontelomeric tagged locus on the same chromosome in the *hdf1* background (ARS607, see Figure S1). Similarly, two other internal loci, ARS1413 and MATα, show no change from their wt distribution upon *hdf1* deletion (A. Taddei, K.D. and S.M.G., unpublished data), and bulk DNA detected by a fluorescent dye remains uniformly distributed (Figure S2).

In contrast to the change observed upon *hdf1* deletion, Tel VI-R remains enriched at the nuclear periphery in the double *mlp1 mlp2* mutant in all phases analyzed (Figure 3A). Again, the average nuclear diameter in GFP-tagged *mlp1 mlp2* cells (∅ = 1.81 μm, n = 124, σ =

A

G1	early S	mIS

obs/random values row 1 (hdf1):
G1: 0.90, 0.98, 1.12
early S: 1.22, 1.06, 0.72
mIS: 1.03, 0.90, 1.07

■ *hdf1*
□ wt

obs/random values row 2 (mlp1mlp2):
G1: 1.96, 0.48, 0.56
early S: 2.08, 0.33, 0.59
mIS: 1.58, 0.65, 0.77

■ *mlp1mlp2*
□ wt

zone: I II III

B

C

D

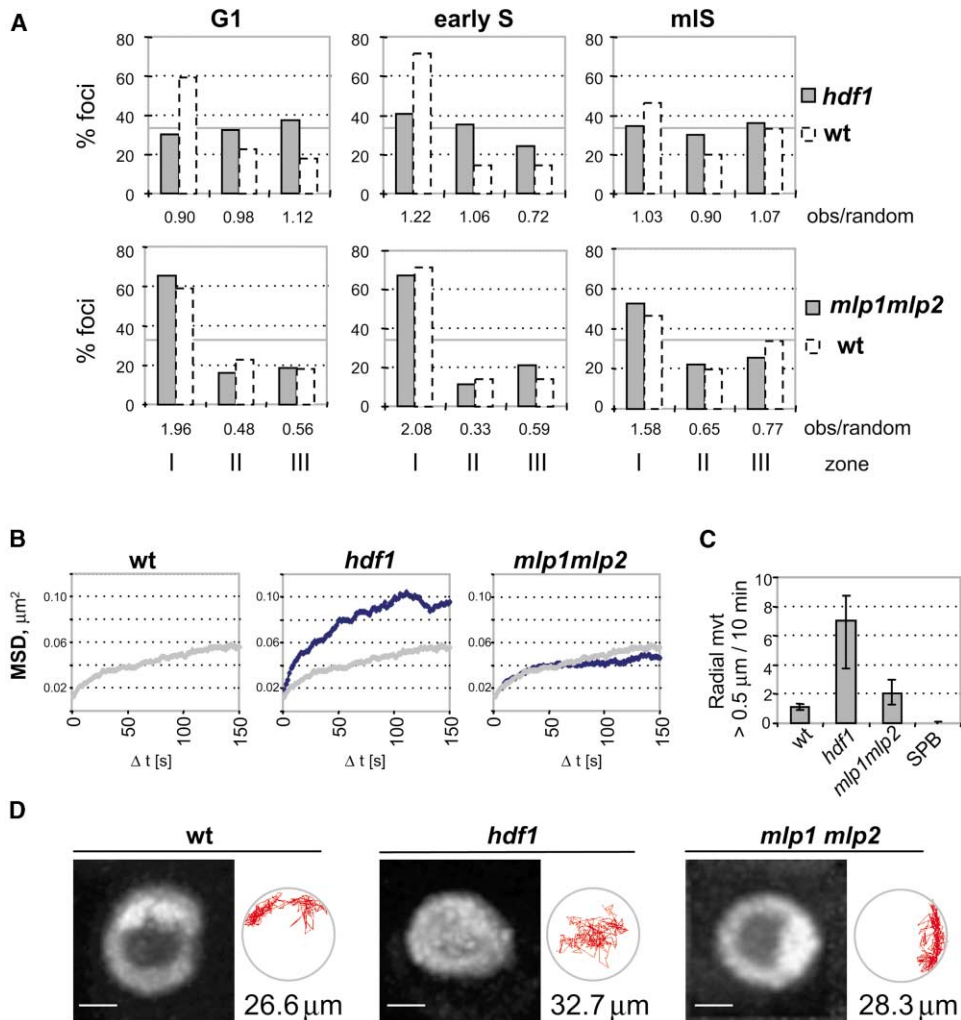wt — 26.6 μm   *hdf1* — 32.7 μm   *mlp1 mlp2* — 28.3 μm

Figure 3. Loss of yKu70p Releases Tel VI-R from the Nuclear Periphery

(A) The position of Tel VI-R with respect to the three concentric zones of the nucleus was determined in wild-type (wt, GA-1459), *hdf1* (GA-1489), and *mlp1 mlp2* (GA-1731) cells as in Figure 1. Gray bars represent *hdf1* or *mlp1 mlp2* mutants, and white bars represent wt (see Figure 1). The number of cells analyzed and the confidence values (p) for the χ^2 analysis between random and test distributions are indicated here in parentheses for each cell cycle stage (G1; eS; mIS): Tel VI-R::*lac*[op] *hdf1* (223, p = 0.41; 54, p = 0.31; 120, p = 0.72); *mlp1 mlp2* (124, p = 3.8×10^{-13}; 61, p = 9.2×10^{-8}; 78, p = 1.4×10^{-3}).

(B) Mean squared displacement analysis was performed by computing the square of the radial displacement of Tel VI-R (measured from the center of the chromosomal tag to the nuclear center) in μm (Δd^2) for time intervals from 0 to 150 s (Δt, seconds): $\Delta d^2 = \{d(t) - d (t + \Delta t)\}^2$. The average of all Δd^2 values for each Δt value is plotted against Δt. The slope is the derivative of the diffusion coefficient, and a plateau indicates spatial constraint. The yeast strains used are shown in (A), and the graphs represent the averages from eight time-lapse series of 300 s each of G1 phase cells. Each curve is calculated from about 1600 measurements. The wt MSD curve is represented in gray in the *hdf1* and *mlp1 mlp2* panels for comparison.

(C) Large radial displacements (>0.5 μm within 10.5 s) were averaged over 40 min of total time-lapse imaging (1.5-s intervals) for the strains used in (A), as well as GA-1987, which carries CFP-Spc42p, a spindle pole body component. The error bars indicate the range of values obtained if large movements are >0.45 μm or >0.55 μm (±10%).

(D) A total of 250 sequential frames of GFP signals (at 1.5-s intervals) in G1 phase cells of the strains indicated in (A) were first aligned based on their nuclear pore signals and were projected on a single image. The absolute position of the Tel VI-R focus was marked by using the AIM tool of the Zeiss LSM 510 software (rel. 2.8). Its trajectory over 5 min is indicated in red on an idealized section of the nucleus, and the mean length averaged over eight movies is indicated. Average error values are wt, σ = 3.3 μm; *hdf1*, σ = 3.7 μm; and *mlp1 mlp2*, σ = 3.3. The scale bar represents 1 μm. The distribution of movement sizes in different strains was compared by using an ANOVA analysis: 29% are >0.2 μm in wt cells, 41% are >0.2 μm in *hdf1* cells, and 32% are >0.2 μm in *mlp1 mlp2* cells.

0.28) is indistinguishable from that measured in wt cells (see above), in contrast to the very large diameters detected for *mlp1 mlp2* nuclei in published FISH studies [30, 37].

To reconcile the lack of change in telomere position documented here for the *mlp1 mlp2* double mutant with the published FISH results, we propose that the double deletion renders nuclei more labile, such that nuclear

integrity and telomere anchoring is lost during the manipulations associated with in situ hybridization. Indeed, we have repeated the Y′ FISH analysis by using double FISH/IF procedures that maintain NE integrity, and, in this case, *mlp1 mlp2* strains retain the peripheral positioning of Y′-containing telomeres [32]. In summary, both FISH and Tel VI-R localization in living cells confirm that the elimination of yKu70, but not of Mlp proteins, leads to a general loss of the perinuclear tethering of yeast Tel VI-R.

Telomeric Micromovements Are Unconstrained in *hdf* Mutants

The random distribution of this telomere at fixed time points in *hdf1* cells could be interpreted either as an enhancement of telomere dynamics or as a redistribution event, which places a subpopulation of Tel VI-R at fixed internal sites. This ambiguity is again readily resolved by time-lapse microscopy, which confirms that individual telomere movement is enhanced in G1 phase nuclei lacking yKu (Figures 3B–3D; see Movie 4 of *hdf1* cells in the Supplementary Material). To compare Tel VI-R dynamics quantitatively, movements were monitored during at least 40 min by using ≥8 different cells of wt, *hdf1*, or *mlp1 mlp2* strains, and dynamics were compared by using three parameters: the freedom of telomere movement or degree of spatial constraint (plotted as mean square displacement or MSD over d(t), [36]), the number of large radial movements per 10 min, and the average distance traveled over a 5-min period [35].

The constraint on telomere movements can be quantified by measuring movement relative to the center of the nuclear sphere, interpolated from the GFP-Nup49 signal on a frame-by-frame basis. The MSD curve achieves a plateau indicating spatial constraint: Tel VI-R movements are nearly identically constrained in wt and *mlp1 mlp2* cells (Figure 3B), while the curve in *hdf1* cells flattens only above 0.08 μm², a value only slightly lower than that calculated for nontelomeric loci in wt cells [35]. We conclude that the loss of yKu, but not of Mlp proteins, reduces constraints on Tel VI-R dynamics (compare Movies 4 and 5 in the Supplementary Material).

An analysis of radial step size shows a near absence of >0.5 μm movements for Tel VI-R in wt interphase nuclei, while, in the *hdf1* mutant, there are, on average, seven per 10 min (Figure 3C). The "released" Tel VI-R is nonetheless more constrained than an internal chromosomal domain in wt (10 ± 3 large movements per 10 min [35]). As a further control that the telomere movement is independent of nuclear rotation or NE deformation, we note that the SPB makes no detectable movement >0.5 μm (Figure 3C).

Absolute dynamics, rather than radial movements, can be shown graphically by projecting Tel VI-R's trajectory during one time-lapse sequence, determined after alignment of nuclear pore signals, onto a single x-y plane (red trace, Figure 3D). Tel VI-R is seen to "sample" a large fraction of the nucleus within 5 min in the *hdf1* mutant, similar to internal chromosomal sites in wt cells [35]. The wild-type Tel VI-R, on the other hand, makes a crescent-shaped track close to the nuclear periphery. When averaged over 40 min for each strain, both the

track length and average step size are shorter in wt cells than in *hdf1* cells (Figure 3 and legend). In contrast, all parameters of Tel VI-R dynamics in the *mlp1 mlp2* strain (position, mean track length, and the average step size) are statistically indistinguishable from the parental values.

Sir-Mediated Repression Improves Perinuclear Anchoring of Native Telomeres

Disruption of either *hdf1* or *hdf2* reduces TPE by 10⁴-fold and provokes the loss of Sir proteins from subtelomeric sequences [8, 25, 26, 29]. Thus, the random distribution of telomeres in an *hdf1* mutant could reflect loss of either a yKu-mediated or a Sir-dependent anchor. To discriminate between these, we tested the localization of Tel VI-R in *sir*-deficient strains and under conditions that increase the efficiency of TPE. The effects on telomeric silencing were scored in the same GFP-tagged strain by integrating a *URA3* reporter fused to [TG$_{1-3}$]$_n$ at Tel VII-L (Table 1).

We find a significant, but incomplete, shift in Tel VI-R position inwards from zone I in strains lacking either *SIR4* or *SIR2* (Figure 4A). Intriguingly, the effects observed in *sir*-deficient cells are most pronounced in early S phase. Again, the random position of an internal *lac*^{op}-tagged site on Chr VI (ARS607) and total DNA density shows no change in distribution in a *sir4* deletion strain (Figures S1 and S2). Unlike Tel VI-R in *hdf1* cells (Figure 3A), its distribution in G1 and eS phase nuclei of *sir2* and *sir4* cells remains slightly nonrandom (Figure 4A). The simplest interpretation of these results is that Sir and yKu proteins act on partially redundant pathways, and that yKu is able to anchor telomeres in the absence of Sir proteins. To test this, Tel VI-R position was determined in the *sir4 hdf1* double mutant and was confirmed as random, similar to the *hdf1* mutant alone (data not shown).

If Sir proteins contribute significantly to telomere tethering, one would expect that telomere anchoring improves as silencing efficiency increases. This has been monitored previously by using artificially truncated telomeres and has yielded contradictory results [16, 37]. To test this correlation at a native telomere, we introduced mutations into the Tel VI-R tagged strain to improve telomeric silencing. Deletion of *RPD3*, which encodes the catalytic subunit of a histone deacetylase complex [38], improves silencing efficiency at telomeres and the mating type loci, possibly due to *SIR3* upregulation (Table 1, [38, 39]). Consistently, the *rpd3* disruption shifts Tel VI-R to an extreme perinuclear position in mid-to-late S phase cells (Figure 4A). This improved anchoring is Sir dependent: the disruption of *sir2* in the *rpd3* strain abolishes the perinuclear enrichment of Tel VI-R, leaving a distribution similar to that in the *sir2* mutant alone (Figure 4A; a statistical comparison between *sir2* and *sir2 rpd3* distributions gives p = 0.30 for G1, p = 0.26 for eS, and p = 0.35 for mlS).

In parallel, we sought to improve repression through the modulation of telomere-associated proteins. By deleting the gene encoding Rif1p, a Rap1 interaction factor that competes for Rap1-Sir protein interactions, we are able to improve TPE (Table 1, [20]). As for the *rpd3*

Table 1. TPE of Mutants Affecting Telomere Localization

Strain	Genotype	Fraction 5-FOA^R	Fold Change
GA-1841	WT	0.51 (0.03–0.78)	1.0
GA-1842	rpd3::LEU2	1.01 (0.63–1.50)	2.0 × up
GA-1844	rpd3::LEU2; sir2::kanMX	<4 × 10^{-6}	1.7 × 10^5 × down
GA-1846	sir2::kanMX	<3 × 10^{-6}	1.7 × 10^6 × down
YG345	hdf1::LEU2	<2 × 10^{-6}	2.6 × 10^5 × down
YG342	hdf1::LEU2; rif1::HIS3	0.07 (0.03–0.11)	7.3 × down
YG526	rif1::TRP1	0.97 (0.57–1.20)	2.0 × up

The frequency of resistance to 5-FOA in strains carrying the *URA3* at a truncated Tel VII-L (*adh4::URA3-Tel*) is shown. The relevant genotypes of the strains are indicated. Repression of *URA3* was determined from a minimum of eight independent colonies by using the standard dilution series assay [40]. The range of values is given in parentheses. For the first four strains, similar changes were scored for efficiency of growth on SD-uracil.

mutant, this shifts Tel VI-R to a more perinuclear distribution in mid-to-late S phase (mlS, Figure 4A). The efficiency of TPE can also be enhanced by the overexpression of Sir3p [19] and can be disrupted by the overexpression of a Sir3 C-terminal fragment [40]. Consistently, Sir3p overexpression improves anchoring in S phase, and elevated levels of the Sir3 C terminus shifts Tel VI-R position inward, such that it resembles that found in *sir2* mutants (Figure S3). Importantly, in all cases in which anchoring improves due to an increase in silencing efficiency, the changes are detected uniquely in S phase. Finally, the immunolocalization of Rap1p and/or Sir4p reveals bright perinuclear foci when silencing is improved, while the proteins are dispersed when silencing is lost (Figure 4B). This establishes a strong correlation between the presence of Sir protein foci, improved telomeric repression, and Tel VI-R anchorage. The cell cycle-restricted penetrance of the phenotype may account for the failure of previous methods to detect it [16].

Recovery of Silencing in the Absence of yKu Restores Anchoring in S Phase Only

The yeast Ku heterodimer and Sir4p interact by two-hybrid analysis [41], and their subtelomeric localization is interdependent: yKu is partially displaced from telomeres in *sir*-deficient strains [29], and the loss of yKu displaces the majority of Sir proteins [8, 24]. Thus, to show unambiguously that silent chromatin itself can anchor telomeres, it was necessary to restore silencing in a yKu-deficient strain. This is possible by creating a double *rif1 hdf1* mutant, as described in Figure 5A [41]. Rif1p competes with Sir proteins for binding to the Rap1 C terminus. Under normal conditions, yKu is thought to help Rap1p recruit Sir4p to telomeres, as the combined Rap1-Sir and yKu-Sir affinities overcome the competition imposed by Rif1p. In the *rif1* mutant, Rap1p recruits Sir4p more efficiently, restoring TPE in the absence of yKu [41]. As previously reported, TPE is restored in the *hdf1 rif1* mutant (Table 1) and correlates with the reappearance of Sir4p foci (Figure 5C), which are lost in *hdf1* strains.

We show here that the perinuclear anchoring of Tel VI-R is fully restored in the double *hdf1 rif1* mutant in S phase (Figure 5B, p values for the comparison of *hdf1 rif1* and wt: p = 1.5 × 10^{-3} for G1, p = 0.42 for eS, and p = 0.31 for mlS). This improved tethering is entirely Sir

dependent (see *hdf1 rif1 sir3* in Figure 5B), although the restored anchorage through Sir proteins is much less efficient in G1 phase than in early or mid-to-late S phase. This establishes unequivocally the existence of a Sir-dependent tethering mechanism that can function independently of yKu. This anchorage pathway correlates in a positive manner with subtelomeric repression and with the presence of Sir protein foci (Figure 5C), while the yKu pathway can function in the absence of TPE.

A Truncated Telomere Is Insensitive to Loss of yKu

Previous results reported little or no change in the position of the truncated Tel VII-L in cells lacking either yKu or Sir3p [16]. To test whether this discrepancy reflects differences in the anchoring of truncated versus native telomeres, we created a similar truncation by integrating a linear fragment containing *ADE2* fused to TG repeats at a unique site between the *lac*^{op} insert and the Tel VI-R subtelomeric repeats (Tel VI-R::*lac*^{op}-*ADE2*-TG, Figure 6A). Using 3D focal stacks analysis, we then compared the position of the truncated Tel VI-R::*lac*^{op}-*ADE2*-TG with the native Tel VI-R position in wt and mutant strains.

The elimination of the subtelomeric X element of Tel VI-R does not significantly alter its perinuclear enrichment in a wt background. In the *hdf1* background, on the other hand, the truncated telomere no longer behaves like the native Tel VI-R (Figure 6C). Notably, Tel VI-R::*lac*^{op}-*ADE2*-TG retains its perinuclear attachment despite the absence of yKu. To confirm that yKu is functionally inactivated in this strain, we monitored TPE of the subtelomeric *ADE2* gene by using a colony color assay (Figure 6B). Indeed, subtelomeric repression of the *ADE2* gene is lost in the strain lacking yKu, producing white rather than sectored colonies.

The persistence of Tel VI-R::*lac*^{op}-*ADE2*-TG anchoring in the absence of yKu suggests that other proteins are efficiently tethering this truncated telomere, despite its low level of silencing. The obvious candidate would be the Sir complex, and, in particular, Sir4p, which was shown to remain telomere bound in the absence of repression [29, 42, 43]. Consistently, by introducing the *sir4 hdf1* double deletion in the truncated Tel VI-R::*lac*^{op}-*ADE2*-TG strain, we find that Tel VI-R is now random in G1 and significantly less well anchored in mid-to-late S phase cells (Figure 6C). Surprisingly, the *sir4* mutation alone is sufficient to delocalize the truncated telomere
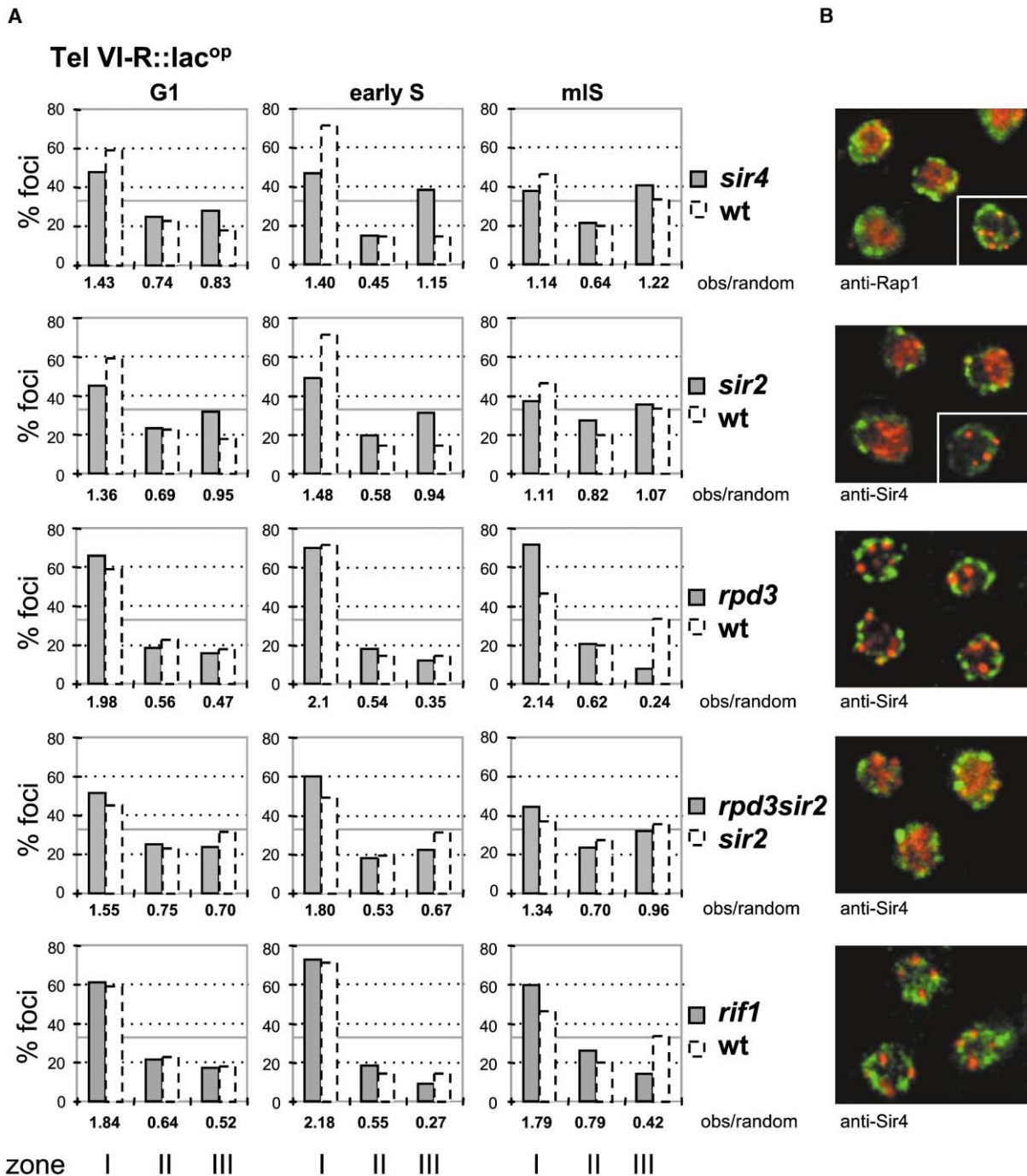
A

Tel VI-R::lac^op

B

Figure 4. Perinuclear Anchoring of Tel VI-R Drops in *sir* Mutants and Correlates with Increased TPE

(A) The position of *lac*^op-tagged Tel VI-R with respect to three concentric zones (see Figure 1) was determined for isogenic strains carrying null alleles for *sir4*, *sir2*, *rpd3*, *rpd3 sir2*, and *rif1* as described in Figure 1. The number of cells analyzed and the confidence values (p) for the χ^2 analysis between random and test distributions are indicated here in parentheses for each strain and cell cycle stage (G1; eS; mIS): Tel VI-R::*lac*^op *sir4* (GA-1867: 358, p = 4.0×10^{-8}; 60, p = 7.8×10^{-3}; 103, p = 3.4×10^{-2}), *sir2* (GA-1846: 135, p = 6.3×10^{-3}; 67, p = 1.1×10^{-2}; 62, p = 0.61), *rpd3* (GA-1842: 129, p = 4.0×10^{-14}; 50, p = 2.4×10^{-7}; 63, p = 5.4×10^{-10}), *rpd3 sir2* (GA-1844: 128, p = 6.8×10^{-5}; 45, p = 7.0×10^{-4}; 94, p = 3.9×10^{-2}), *rif1* (GA-1793: 289, p = 6.9×10^{-23}; 44, p = 1.6×10^{-7}; 114, p = 5.3×10^{-9}).

(B) Immunolocalization of Sir4p (red) and nuclear pore (Mab414, green) were performed in the *sir2*, *rpd3*, *rpd3 sir2*, and *rif1* strains (see the Experimental Procedures). For the *sir4* deletion strain, the staining in red is with affinity purified anti-Rap1p. The same staining in a wt strain is shown in the inset. In all cases, the appearance of foci correlates with improved or normal repression, while diffuse staining indicates loss of silencing.

A

B

C
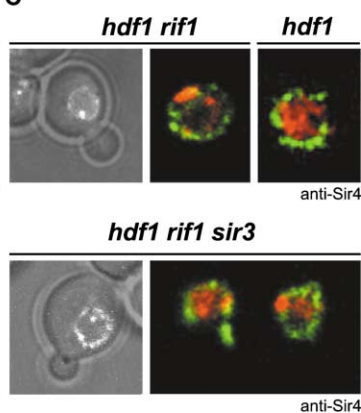

anti-Sir4

anti-Sir4
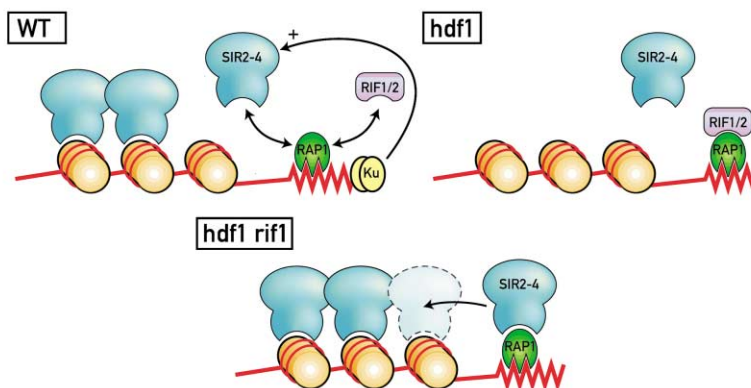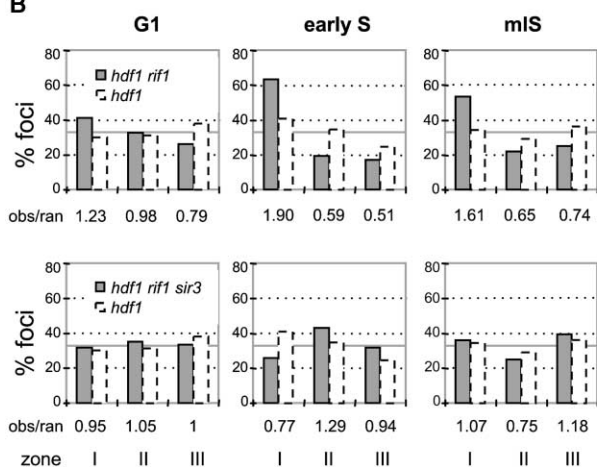
Figure 5. yKu-Independent Anchoring by Sir Proteins

(A) In wild-type cells, yKu helps Rap1p recruit Sir proteins, overcoming competition from Rif1/2p. In the absence of yKu, a *rif1* deletion restores TPE by eliminating the competition for Sir binding to the Rap1 C-terminal tail (*hdf1 rif1*).

(B) The position of *lac*op-tagged Tel VI-R with respect to three concentric zones (Figure 1) was determined for isogenic wt, *hdf1*, *hdf1 rif1*, and *hdf1 rif1 sir3* strains as in Figure 1. Gray bars and the enrichment or depletion relative to a random distribution represent values for the *hdf1 rif1* and *hdf1 rif1 sir3* mutants. The *hdf1* strain is presented in white (see Figure 3). The number of cells analyzed and the confidence values (p) for the χ^2 analysis between random and test distributions are indicated here in parentheses for each strain and cell cycle stage (G1; eS; mIS): Tel VI-R::*lac*op, *hdf1 rif1* (GA-1794: 267, p = 1.1×10^{-2}; 41, p = 2.3×10^{-4}; 129, p = 6.9×10^{-6}), and *hdf1 rif1 sir3* (GA-1866: 129, p = 0.91; 35, p = 0.45; 56, p = 0.40).

(C) Characteristic phase-GFP images of the analyzed cells are shown to the left, and anti-Sir4p localization coupled with Mab414 staining of nuclear pores is shown to the right for the indicated mutants.

from the nuclear periphery in S phase, while it does not have the same effect on the native Tel VI-R. Thus, while native and truncated telomeres exploit the same two anchoring pathways, subtelomeric context appears to influence the degree to which anchorage is dependent on yKu or Sir4p.

Anchoring Pathway Dominance Varies among Native Telomeres

To see if other native telomeres also show variability in the degree to which the yKu- or the Sir-dependent pathway dominates, we examined the positioning of Tel VIII-L and Tel XIV-L in various single and double mutants. Tel VIII-L, being less efficiently anchored to begin with,

becomes randomly distributed upon deletion of *hdf1* alone, like Tel VI-R (Figure S4). Tel XIV-L, on the other hand, shows a significant drop in its perinuclear enrichment in G1 phase upon elimination of the yKu anchor but remains strongly tethered in S phase cells (Figure 6D). Importantly, deletion of *sir4* alone leads to a more significant loss of anchoring than deletion of *hdf1*, and the double *sir4 hdf1* deletion is required to render Tel XIV-L fully random in both G1 and S phase cells (Figure 6D, see p values in legend). Thus, Tel XIV-L positioning at the NE is again both yKu and Sir dependent, the S phase character of Sir-mediated anchoring is maintained, yet the relative importance of the two pathways is different from that shown for Tel VI-R. A model de-
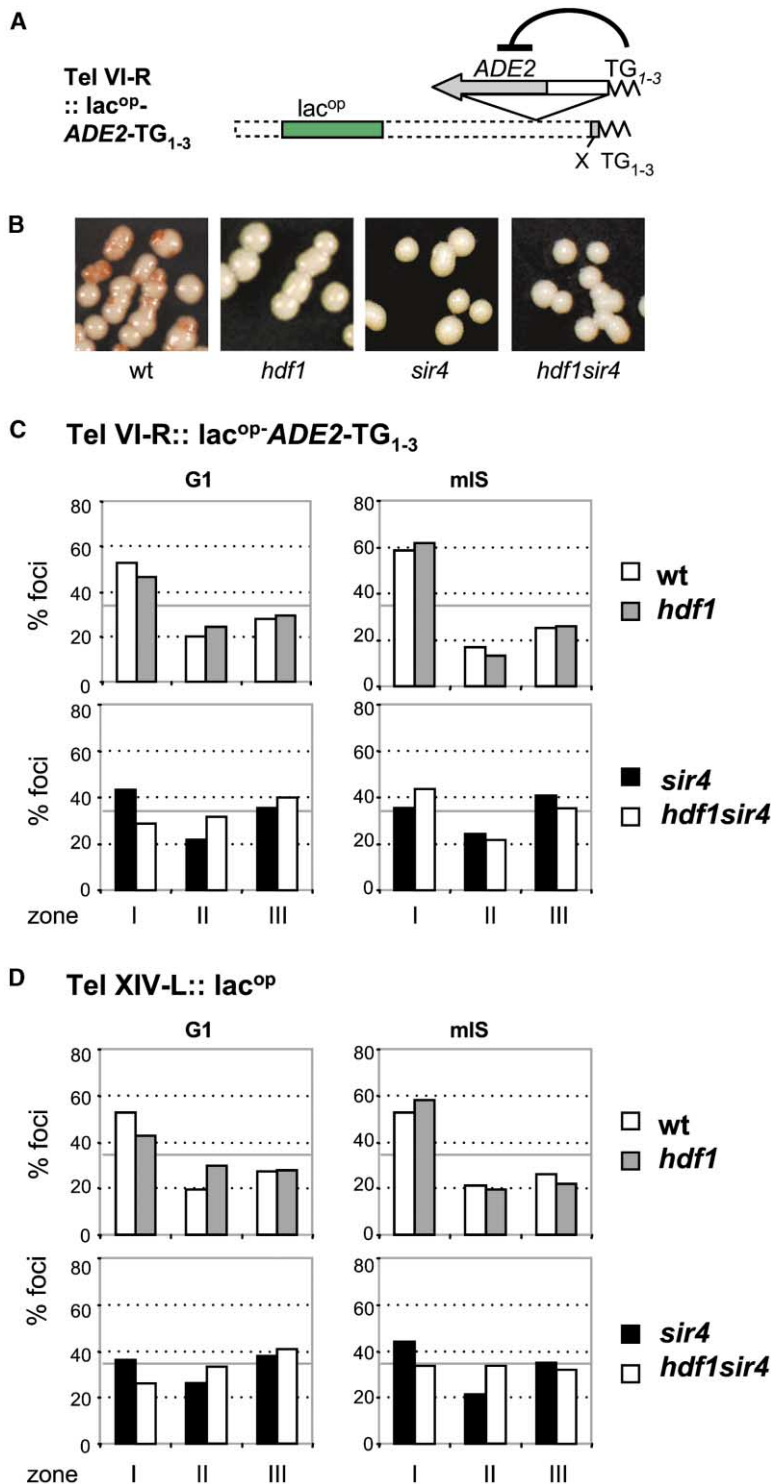
A

Tel VI-R
:: lac^op-
ADE2-TG$_{1-3}$

B

wt   *hdf1*   *sir4*   *hdf1sir4*

C   Tel VI-R:: lac^op-*ADE2*-TG$_{1-3}$

G1   mIS

□ wt
■ *hdf1*

■ *sir4*
□ *hdf1sir4*

zone   I   II   III

D   Tel XIV-L:: lac^op

G1   mIS

□ wt
■ *hdf1*

■ *sir4*
□ *hdf1sir4*

zone   I   II   III

Figure 6. yKu- and Sir-Dependent Pathways Contribute Differentially to Anchoring

(A) The *lac^op*-tagged Tel VI-R (GA-1459) was truncated at 5 kb from the native chromosomal end, centromere-proximal of the last coding sequence (YFR057W), by integration of *ADE2* and $\sim$100 bp of [TG$_{1-3}$]$_n$. This creates a telomere lacking all subtelomeric repeat elements and allows monitoring of TPE through the *ADE2* color assay.

(B) Colonies of the indicated strain bearing a truncated Tel VI-R are grown on limiting adenine to monitor the presence (sectored) or absence (white) of TPE.

(C) The subnuclear position of the truncated Tel VI-R was determined in wt, *hdf1, sir4,* and *hdf1 sir4* strains as in Figure 1. The strain number, the number of cells analyzed, and the confidence values (p) for the χ^2 analysis between random and test distributions are indicated in parentheses for each cell cycle stage (G1; mIS) of strains carrying Tel VI-R:: *lac^op*-ADE2-TG: wt (GA-1917: 431, p = 6.4 $\times$ 10^{-17}; 140, p = 8.9 $\times$ 10^{-10}), *hdf1* (GA-1918: 227, p = 7.3 $\times$ 10^{-5}; 101, p = 4.9 $\times$ 10^{-9}), *sir4* (GA-2067: 303, p = 3.0 $\times$ 10^{-5}; 79, p = 0.19); *sir4 hdf1* (GA-2068: 207, p = 0.10; 131, p = 7.4 $\times$ 10^{-3}).

(D) The subnuclear position of Tel XIV-L was determined in wt, *hdf1, sir4,* and *hdf1 sir4* strains as in Figure 1. The strain number, the number of cells analyzed, and the confidence values (p) for the χ^2 analysis between random and test distributions are indicated in parentheses for each cell cycle stage (G1; mIS) of strains carrying Tel XIV-L::*lac^op*: wt (GA-1985: 257, p = 8.1 $\times$ 10^{-11}; 89, p = 4.4 $\times$ 10^{-4}), *hdf1* (GA-1983: 198, p = 2.4 $\times$ 10^{-2}; 72, p = 4.9 $\times$ 10^{-9}), *sir4* (GA-2113: 292, p = 3.9 $\times$ 10^{-2}; 66, p = 7.5 $\times$ 10^{-2}), *hdf1sir4* (GA-2114: 272, p = 1.2 $\times$ 10^{-2}; 94, p = 9.6 $\times$ 10^{-1}).

scribing the two partially redundant pathways and the behavior of the native Tel VI-R in G1 and S phases is presented in Figure 7.

Discussion

Time-lapse microscopy documents a significant level of chromatin movement within the nuclei of yeast, flies, and human cells, both as short-range, saltatory motion and long-range, chromosomal migration [1, 35, 36, 44, 45]. The clustering of yeast telomeres near the nuclear envelope, on the other hand, appears to define a relatively stable subnuclear compartment that favors chromatin-mediated repression [2]. Here, we show by time-lapse microscopy that individual native telomeres can be highly dynamic, moving significantly more than an

Ku70/80

Sir2/3/4

Rap1p

Nucleosomes

Subtelomeric repeats

wt   *hdf1 rif1*   wt   *hdf1 rif1*

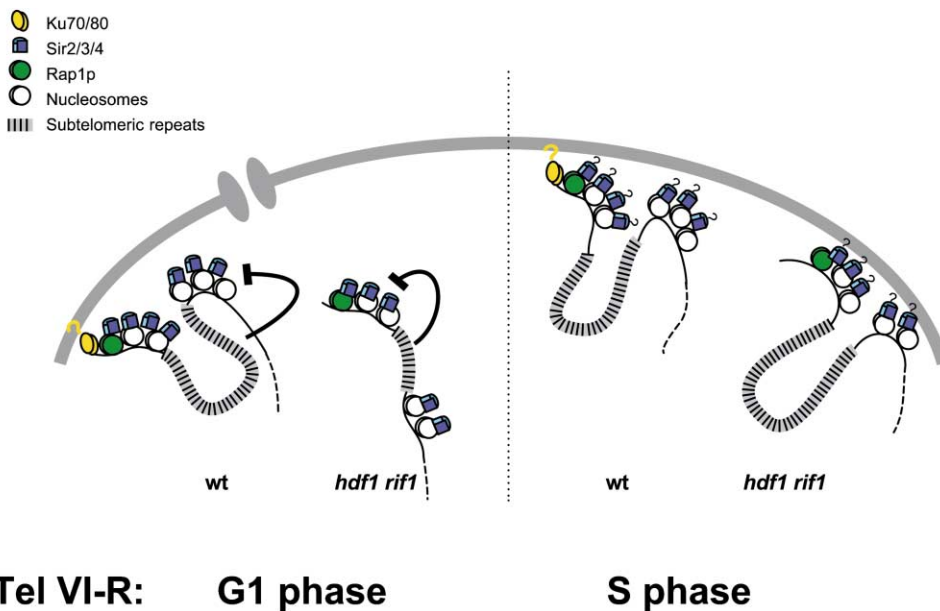## Tel VI-R: G1 phase   S phase

Figure 7. Cell Cycle Variation in the Redundant Anchoring Mechanisms of Yeast Telomeres

During G1 phase in wild-type (wt) cells, the yKu-mediated pathway is necessary for native Tel VI-R anchoring, suggesting that the Sir-mediated pathway is inactive. yKu-mediated anchoring of native telomeres does not depend on the presence of Mlp1/2 proteins. The analysis of a strain deficient for yKu and Rif1p (*hdf1 rif1*) reveals the Sir-mediated anchoring pathway, which is functional in S phase, but not in G1 phase. We propose that the subtelomeric repeats directly or indirectly impair the ability of Sir proteins to anchor native ends in G1 phase.

integral NE component like the spindle pole body. Telomeres, nonetheless, remain confined within a peripheral zone in interphase nuclei of ~0.2 μm in width, a degree of confinement more pronounced than that described for *lac*[op]-tagged domains at the nuclear periphery in mammalian nuclei [45]. This behavior is highly suggestive of rapidly reversible interactions between the telomere and redundant membrane-associated binding sites. Such interactions could effectively "cage" a telomere at the nuclear periphery.

The End Binding Complex yKu and Silent Chromatin Define Redundant Anchoring Pathways

We have uncovered two partially redundant pathways for yeast telomere anchorage: one is dependent on the heterodimeric yKu complex, and the second is dependent on the histone binding Sir repressor complex. Mutants that restore TPE in the absence of yKu show unambiguously that there is a significant Sir-dependent anchor that functions independently of yKu at native Tel VI-R (Figure 5). Because both yKu and Sir complexes bind telomeres in vivo [26, 29, 43], and because neither mutation affects the subnuclear distribution of internal chromosomal loci, our data strongly implicate yKu and the Sir complex directly in telomere anchoring.

The yKu pathway is able to anchor some telomeres throughout interphase, even in the complete absence of Sir proteins and subtelomeric repression. The Sir-dependent pathway, on the other hand, correlates with chromatin-mediated transcriptional repression and functions most efficiently in S phase. The redundancy of these pathways, and the fact that they can function

with different efficiencies at different chromosomal ends, accounts for much of the contradictory data reported on yeast telomeric anchoring [10, 16, 24, 30, 37]. By extending our analysis to several native and truncated ends, our data suggest that these dual pathways account for most telomere tethering in yeast.

In contrast to published results [30, 37], we show here that the absence of the two nuclear Myosin-like proteins, Mlp1 and Mlp2, which were proposed to form the bridge between yKu and nuclear pores, has no significant impact on telomere positioning or on their short-range dynamics. These results are reinforced by the observation that TPE is fully intact and Sir proteins are not displaced from telomeres in the *mlp1 mlp2* double mutant [32]. Because neither yKu nor Sir proteins are inherently membrane-associated, and because yeast lacks nuclear lamins, it seems obvious that some component of the NE will be implicated in the anchoring mechanism. One candidate that may replace lamin as a chromatin anchor is the Enhancer of silent chromatin protein 1, a polypeptide located at the yeast nuclear periphery that is necessary for the stable mitotic partitioning of a Sir4-bound plasmid [46].

Telomere anchoring is not the only function of the inner nuclear envelope. Perinuclear binding sites in G1 have been shown to correlate with late-firing origins of replication [33], and artificial tethering to nuclear pores may be able to provide boundary function [47]. The inner nuclear envelope is likely to have subzones defined by the presence of different structural proteins. It is possible that nuclear pores and/or Mlp proteins play a role in the demarcation of such subdomains, accounting for the reported disruption of nuclear organization detected in *nup60* or *nup145* pore mutants [37].

Subtelomeric Repeats Provide "Antisilencing" and "Antianchor" Functions

Our data show that subtelomeric sequence organization influences anchorage mechanisms by influencing the relative importance of the yKu- and the Sir-mediated anchorage pathways. Notably, the native Tel VI-R end is displaced from the nuclear periphery throughout the cell cycle in an *hdf1* deletion, while the anchorage of Tel XIV-L is reduced only in G1 phase. Even in G1 phase, Tel XIV-L does not become fully random unless the Sir-dependent pathway is also compromised (Figure 6D). Similarly, Tel XIV-L remains anchored in S phase in the absence of yKu, through a pathway that is entirely Sir-dependent (Figure 6). These results suggest that native telomeres will vary considerably in the degree to which they are released by an *hdf1* deletion. This is consistent with data showing that native telomeres are dere-pressed to different degrees in an *hdf1* background [13, 14] and that Y′ FISH analysis delocalizes only 50% of native ends [8]. We previously reported that a heritable epigenetic state can suppress the delocalization of telomeres in an *hdf1* mutant [24]. This current study suggests that the heritable state is likely to be Sir depen-dent. In addition, the amount of the internal $[TG_{1-3}]_n$ repeat at a native telomere may correlate inversely with the telomere's sensitivity to *hdf* mutations, since Rap1, like yKu, serves to nucleate Sir complex binding [29, 41].

Consistent with data from Tham et al. [16], we find that a truncated telomere is not released from the pe-riphery in an *hdf1* mutant. However, here we show that the anchoring of the truncated telomere is Sir4 de-pendent, since complete delocalization is achieved in the double *hdf1 sir4* mutant (Figure 6C). Both chroma-tin immunoprecipitation and one-hybrid assays in *hdf1* and *sir3* cells show that Sir4p remains associated with $[TG_{1-3}]_n$ repeats in the absence of TPE [29, 42, 43]. This silencing-independent association of Sir4p may be suffi-cient to tether a truncated end, although it is ineffective for the native Tel VI-R. Alternatively, Sir4p may provide a kind of cross-tether to keep the truncated end associ-ated with another native telomere that is itself *hdf1* in-sensitive. Strains that allow us to monitor intertelomere interactions will be required to address this possibility.

To account for the differential effects of *hdf1* deletion on artificial and native Tel VI-R, we suggest that some subtelomeric sequences counteract the Sir-dependent tethering pathway in G1 phase (Figure 7). Indeed, X elements cause an abrupt drop in the propagation of TPE [13, 14]. By limiting the amount of Sir proteins bound, the X elements may have an "antianchor" effect, rendering native Tel VI-R position sensitive to the loss of yKu.

Is Anchoring a Cause or Result of Transcriptional Repression?

In the *hdf1 rif1* double mutant, we show that the Sir pathway can efficiently restore native end attachment, but only in S phase (Figure 5). This, and the release of telomeres in G2/M, demonstrates that subnuclear positioning is cell cycle regulated. The S phase varia-tions correlate well with results showing that passage through S phase, but not DNA replication, is necessary to establish Sir repression [48, 49].

It is often asked whether subnuclear positioning is the cause or the result of changes in gene expression. The dual pathways elucidated here suggest that both are true in yeast. The silencing-independent tethering through yKu brings telomeres to a peripheral zone of reduced volume, prior to or independent of a repressed chromatin state. The resulting local concentration of Rap1p binding sites may attract sufficiently high con-centrations of Sir proteins to nucleate assembly onto adjacent nucleosomes. Anchorage by yKu would thus precede and promote nucleation of the repressed chro-matin.

More to the point, however, is the demonstration that Sir proteins themselves can tether native telomeres in a manner correlated with increased repression. If silent chromatin can itself promote association with the NE, then subnuclear positioning is a consequence of gene repression, as well as a cause. We predict that Sir-dependent anchoring may be of particular importance for its mitotic inheritance by promoting the juxtaposition of repressed domains in the newly formed nuclei at telophase.

Conclusions

Specific subnuclear positioning and long-range interac-tion between heterochromatic domains occurs in nearly all plant and animal species. In differentiated cells, het-erochromatin is found adjacent to the nuclear lamina, yet it is unclear what mechanisms target chromatin to specific nuclear sites. We show here that the perinuclear anchoring of telomeres in yeast is mediated by two re-dundant pathways requiring, respectively, yKu and the Silent information regulatory complex. The fact that an-chorage correlates with repression and Sir binding sug-gests that the subnuclear position of silent chromatin may be self-determined, through its affinity for nuclear envelope components.

Experimental Procedures

Plasmid, Strains, and Yeast Methods

Culture conditions, media, and repression assays were performed as described [40]. Integration of 6–10 kb of multimerized *lac* opera-tors [34] at unique sequences close to telomeres (14 kb from Tel VI-R, 19 kb from Tel VIII-L, and 11 kb from Tel XIV-L) into GA-1320 [33] gave rise to GA-1459, GA-1986, and GA-1985, respectively. Gene deletion was performed by using a PCR-based gene deletion technique with primers that were within 100 bp of the beginning and end of each gene [50], resulting in complete null alleles of *hdf1*, *mlp1*, *mlp2*, *sir4*, *sir2*, and *rif1*, which were checked by PCR and Southern analyses. The *rpd3::LEU2* and *sir3::LEU2* disruption used published plasmids [38, 40]. GA-1987 was obtained by inserting *SPC42-CFP::URA3* into GA-1985, and Tel VI-R truncation was ob-tained by integration of pFH1 (containing a 1-kb *AccI* fragment downstream of YFR055W, the *ADE2* gene, and $[TG_{1-3}]$ repeats) into GA-1459. All strains used are indicated in Table S1, available in the Supplementary Material.

IF and Live Fluorescence Microscopy

For immunofluorescence assays, cells were fixed prior to sphero-plasting and were reacted with affinity-purified rabbit antisera whose specificities have been previously characterized [7, 10] or with the antipore monoclonal MAb414 (BABCO).

For live imaging, cultures were grown in SD-histidine, to a concen-tration of less than 1×10^7 cells/ml. Live microscopy was performed between 22°C and 25°C. Cells were spread on SD-histidine agar patches containing 4% glucose, and 19-image stacks with a 170

nm step size were captured on a Tillvision driven Olympus IX70 microscope as described [33]. Phase images were taken to assign cell cycle stages, which were classified as follows: unbudded cells = G1 phase, very small budded cells = early S phase (eS), budded cells in which the bud is big enough to form a ring at the bud neck and the nucleus is still round = mid-to-late S phase (mlS). Once the nucleus moves to the bud neck and begins to deform, the cells were considered to be in G2/M. Time-lapse imaging was performed with a Zeiss LSM510 confocal microscope as described [35], except that a 100× Planapo objective was used at zoom level 2 (90 nm/pixel).

Quantitative Analyses of Position and Dynamics
The position of the GFP spot is determined by measuring the spot-to-periphery distance and the nuclear diameter (perimeter is defined as the middle of the Nup49-GFP ring). By dividing the first by the second, each spot falls into one of the three concentric zones of equal surface (see Figure 1B). The most peripheral zone I has a width of 0.184 × the nuclear radius (r), zone II = 0.184 × r to 0.422 × r, and zone III has a radius of 0.422 × r. Measurements were performed with Tillvision 4.0 imaging software (TILL Photonics). Time-lapse 2D images were analyzed in an automated fashion relative to the calculated nuclear center with MetaMorph Offline v 4.6r6 (Universal Imaging). Radial movements were calculated by plotting spot-to-center or spot-to-pore distances relative to time, and large radial movements were scored as moves >0.5 μm within 10.5 s and are averaged over 10 min [35]. MSD analysis was performed as described [35, 36].

For each strain analyzed for rapid movement, usually one or two out of eight time-lapse series (300 s each) are atypical. No deviant examples were suppressed, although this frequency suggests that they reflect an as yet unidentified change in cellular physiology. The induction of DNA damage by bleomycin correlates with enhanced telomere movement; thus, it possible that, in ∼10% of the cells, physiological or laser-induced damage provokes telomere movement.

Statistics and Error Estimation
Distributions of tagged telomere position were compared either to the predicted random array with a χ^2 analysis or to another distribution with the latter proportional analysis comparing zone I percentages. Statistical significance was determined by using a 95% confidence interval.

Supplementary Material
Supplementary Material is available at http://images.cellpress.com/ supmat/supmatin.htm. This includes examples of time-lapse series of Tel VI-R-associated GFP signals of either a wild-type, an *hdf1* deletion, or an *mlp1 mlp2* deletion strain, with examples from wild-type cells in G1, S, and G2/M phases. Also shown is the distribution of an internal GFP-tagged locus, ARS607, and bulk DNA in wt, *hdf1*, and *sir4* strains, and the changes in Tel VI-R position correlated with the overexpression of Sir3p or the Sir3 C terminus. Finally, the effects of *hdf1* deletion on GFP-tagged Tel VIII-L are quantified by using 3D stacks of living cells.

References

1. Marshall, W.F. (2002). Order and disorder in the nucleus. Curr. Biol. *12*, R185–R192.
2. Cockell, M., and Gasser, S.M. (1999). Nuclear compartments and gene regulation. Curr. Opin. Genet. Dev. *9*, 199–205.
3. Fisher, A.G., and Merkenschlager, M. (2002). Gene silencing, cell fate and nuclear organisation. Curr. Opin. Genet. Dev. *12*, 193–197.
4. Gottschling, D.E., Aparicio, O.M., Billington, B.L., and Zakian, V.A. (1990). Position effect at *S. cerevisiae* telomeres: reversible repression of Pol II transcription. Cell *63*, 751–762.
5. Nimmo, E.R., Cranston, G., and Allshire, R.C. (1994). Telomere-associated chromosome breakage in fission yeast results in variegated expression of adjacent genes. EMBO J. *13*, 3801–3811.
6. Funabiki, H., Hagan, I., Uzawa, S., and Yanagida, M. (1993). Cell cycle-dependent specific positioning and clustering of centromeres and telomeres in fission yeast. J. Cell Biol. *121*, 961–976.
7. Palladino, F., Laroche, T., Gilson, E., Axelrod, A., Pillus, L., and Gasser, S.M. (1993). SIR3 and SIR4 proteins are required for the positioning and integrity of yeast telomeres. Cell *75*, 543–555.
8. Laroche, T., Martin, S.G., Gotta, M., Gorham, H.C., Pryde, F.E., Louis, E.J., and Gasser, S.M. (1998). Mutation of yeast Ku genes disrupts the subnuclear organization of telomeres. Curr. Biol. *8*, 653–656.
9. Laroche, T., Martin, S.G., Tsai-Pflugfelder, M., and Gasser, S.M. (2000). The dynamics of yeast telomeres and silencing proteins through the cell cycle. J. Struct. Biol. *129*, 159–174.
10. Gotta, M., Laroche, T., Formenton, A., Maillet, L., Scherthan, H., and Gasser, S.M. (1996). The clustering of telomeres and colocalization with Rap1, Sir3, and Sir4 proteins in wild-type *Saccharomyces cerevisiae*. J. Cell Biol. *134*, 1349–1363.
11. Scherf, A., Figueiredo, L.M., and Freitas-Junior, L.H. (2001). Plasmodium telomeres: a pathogen's perspective. Curr. Biol. *4*, 409–414.
12. Pryde, F.E., Gorham, H.C., and Louis, E.J. (1997). Chromosome ends: all the same under their caps. Curr. Opin. Genet. Dev. *7*, 822–828.
13. Pryde, F.E., and Louis, E.J. (1999). Limitations of silencing at native yeast telomeres. EMBO J. *18*, 2538–2550.
14. Fourel, G., Revardel, E., Koering, C.E., and Gilson, E. (1999). Cohabitation of insulators and silencing elements in yeast subtelomeric regions. EMBO J. *18*, 2522–2537.
15. Cryderman, D.E., Morris, E.J., Biessmann, H., Elgin, S.C., and Wallrath, L.L. (1999). Silencing at *Drosophila* telomeres: nuclear organization and chromatin structure play critical roles. EMBO J. *18*, 3724–3735.
16. Tham, W.H., Wyithe, J.S., Ferrigno, P.K., Silver, P.A., and Zakian, V.A. (2001). Localization of yeast telomeres to the nuclear periphery is separable from transcriptional repression and telomere stability functions. Mol. Cell *8*, 189–199.
17. Andrulis, A.D., Neiman, A.M., Zappulla, D.C., and Sternglanz, R. (1998). Perinuclear localization of chromatin facilitates transcriptional silencing. Nature *394*, 592–595.
18. Gartenberg, M.R. (2000). The Sir proteins of *S. cerevisiae*: mediators of transcriptional silencing and much more. Curr. Opin. Microbiol. *3*, 132–137.
19. Renauld, H., Aparicio, O.M., Zierath, P.D., Billington, B.L., Chhablani, S.K., and Gottschling, D.E. (1993). Silent domains are assembled continuously from the telomere and are defined by promoter distance and strength, and by SIR3 dosage. Genes Dev. *7*, 1133–1145.
20. Buck, S.W., and Shore, D. (1995). Action of a RAP1 carboxy-terminal silencing domain reveals an underlying competition between HMR and telomeres in yeast. Genes Dev. *9*, 370–384.
21. Maillet, L., Boscheron, C., Gotta, M., Marcand, S., Gilson, E., and Gasser, S.M. (1996). Evidence for silencing compartments within the yeast nucleus: a role for telomere proximity and Sir protein concentration in silencer-mediated repression. Genes Dev. *10*, 1796–1811.
22. Thompson, J.S., Johnson, L.M., and Grunstein, M. (1994). Specific repression of the yeast silent mating locus HMR by an adjacent telomere. Mol. Cell. Biol. *14*, 446–455.

23. Marcand, S., Buck, S.W., Moretti, P., Gilson, E., and Shore, D. (1996). Silencing of genes at nontelomeric sites in yeast is controlled by sequestration of silencing factors at telomeres by Rap 1 protein. Genes Dev. *10*, 1297–1309.

24. Maillet, L., Gaden, F., Brevet, V., Fourel, G., Martin, S.G., Dubrana, K., Gasser, S.M., and Gilson, E. (2001). Ku-deficient strains exhibit alternative states of silencing competence. EMBO Rep. *3*, 203–210

25. Shore, D. (1998). Telomeres–unsticky ends. Science *281*, 1818–1819.

26. Critchlow, S.E., and Jackson, S.P. (1998). DNA end-joining: from yeast to man. Trends Biochem. Sci. *23*, 394–398.

27. Gravel, S., Larrivee, M., Labrecque, P., and Wellinger, R.J. (1998). Yeast Ku as a regulator of chromosomal DNA end structure. Science *280*, 741–744.

28. Peterson, S.E., Stellwagen, A.E., Diede, S.J., Singer, M.S., Haimberger, Z.W., Johnson, C.O., Tzoneva, M., and Gottschling, D.E. (2001). The function of a stem-loop in telomerase RNA is linked to the DNA repair protein Ku. Nat. Genet. *27*, 64–67.

29. Martin, S.G., Laroche, T., Suka, N., Grunstein, M., and Gasser, S.M. (1999). Relocalization of telomeric Ku and SIR proteins in response to DNA strand breaks in yeast. Cell *97*, 621–633.

30. Galy, V., Olivo-Marin, J.C., Scherthan, H., Doye, V., Rascalou, N., and Nehrbass, U. (2000). Nuclear pore complexes in the organization of silent telomeric chromatin. Nature *403*, 108–112.

31. Strambio-de-Castillia, C., Blobel, G., and Rout, M.P. (1999). Proteins connecting the nuclear pore complex with the nuclear interior. J. Cell Biol. *144*, 839–855.

32. Hediger, F., Dubrana, K., and Gasser, S.M. (2002). Myosin-like proteins 1 and 2 are not required for silencing or telomere anchoring, but act in the Tel1 pathway of telomere length control. J. Struct. Biol. *140*, 79–91.

33. Heun, P., Laroche, T., Raghuraman, M.K., and Gasser, S.M. (2001). The positioning and dynamics of origins of replication in the budding yeast nucleus. J. Cell Biol. *152*, 385–400.

34. Straight, A.F., Belmont, A.S., Robinett, C.C., and Murray, A.W. (1996). GFP tagging of budding yeast chromosomes reveals that protein-protein interactions can mediate sister chromatid cohesion. Curr. Biol. *6*, 1599–1608.

35. Heun, P., Laroche, T., Shimada, K., Furrer, P., and Gasser, S.M. (2001). Chromosome dynamics in the yeast interphase nucleus. Science *294*, 2181–2186.

36. Marshall, W.F., Straight, A., Marko, J.F., Swedlow, J., Dernburg, A., Belmont, A., Murray, A.W., Agard, D.A., and Sedat, J.W. (1997). Interphase chromosomes undergo constrained diffusional motion in living cells. Curr. Biol. *7*, 930–939.

37. Feuerbach, F., Galy, V., Trelles-Sticken, E., Fromont-Racine, M., Jacquier, A., Gilson, E., Olivo-Marin, J.C., Scherthan, H., and Nehrbass, U. (2002). Nuclear architecture and spatial positioning help establish transcriptional states of telomeres in yeast. Nat. Cell Biol. *4*, 214–221.

38. Rundlett, S.E., Carmen, A.A., Kobayashi, R., Bavykin, S., Turner, B.M., and Grunstein, M. (1996). HDA1 and RPD3 are members of distinct yeast histone deacetylase complexes that regulate silencing and transcription. Proc. Natl. Acad. Sci. USA *93*, 14503–14508.

39. Sun, Z.W., and Hampsey, M. (1999). A general requirement for the Sin3-Rpd3 histone deacetylase complex in regulating silencing in *S. cerevisiae*. Genetics *152*, 921–932.

40. Gotta, M., Palladino, F., and Gasser, S.M. (1998). Functional characterization of the N terminus of Sir3p. Mol. Cell. Biol. *18*, 6110–6120.

41. Mishra, K., and Shore, D. (1999). Yeast Ku protein plays a direct role in telomeric silencing and counteracts inhibition by Rif proteins. Curr. Biol. *9*, 1123–1126.

42. Bourns, B.D., Alexander, M.K., Smith, A.M., and Zakian, V.A. (1998). Sir proteins, Rif proteins, and Cdc13p bind *Saccharomyces* telomeres in vivo. Mol. Cell. Biol. *18*, 5600–5608.

43. Luo, K., Vegas-Palas, M.A., and Grunstein, M. (2002). Rap1-Sir4 bindingindependent of other Sir, yKu or histone interactions initiates the assembly of telomeric heterochromatin in yeast. Genes Dev. *16*, 1528–1539.

44. Vazquez, J., Belmont, A.S., and Sedat, J.W. (2001). Multiple regimes of constrained chromosome motion are regulated in the interphase *Drosophila* nucleus. Curr. Biol. *11*, 1227–1239.

45. Chubb, J.R., Boyle, S., Perry, P., and Bickmore, W.A. (2002). Chromatin motion is constrained by association with nuclear compartments in human cells. Curr. Biol. *12*, 439–445.

46. Andrulis, E.D., Zappulla, D.C., Ansari, A., Perrod, S., Laiosa, C.V., Gartenberg, M.R., and Sternglanz, R. (2002). Esc1, a nuclear periphery protein required for Sir4-based plasmid anchroing and partitioning. Mol. Cell. Biol. *22*, 8292–8301.

47. Ishii, K., Arib, G., Lin, C., Van Houwe, G., and Laemmli, U.K. (2002). Chromatin boundaries in budding yeast. The nuclear pore connection. Cell *109*, 551–562.

48. Li, Y.C., Cheng, T.H., and Gartenberg, M.R. (2001). Establishment of transcriptional silencing in the absence of DNA replication. Science *291*, 650–653.

49. Kirchmaier, A.L., and Rine, J. (2001). DNA replication-independent silencing in *S. cerevisiae*. Science *291*, 646–650.

50. Longtine, M.S., McKenzie, A., 3rd, Demarini, D.J., Shah, N.G., Wach, A., Brachat, A., Philippsen, P., and Pringle, J.R. (1998). Additional modules for versatile and economical PCR-based gene deletion and modification in *S. cerevisiae*. Yeast *14*, 953–961.